Detection and quantification of copper in scrap metal by linac-based neutron activation analysis

Adrien Sari, Sara Garti, Frédéric Lainé, Hamid Makil, Nicolas Dufour, Romuald Woo, Frédérick Carrel, Philippe Russo

Detection and quantification of copper in scrap metal by linac-based neutron activation analysis

Adrien Sari[1], Sara Garti[1], Frédéric Lainé[1], Hamid Makil[1], Nicolas Dufour[1], Romuald Woo[1], Frédérick Carrel[1], Philippe Russo[2]

[1]CEA, LIST, Laboratoire Capteurs et Architectures Electroniques, 91191 Gif-sur-Yvette Cedex, France

[2]ArcelorMittal, Global Research and Development, Maizières Process, F-57283 Maizières-lès-Metz Cedex, France

*Corresponding author: Adrien Sari (tel.: +33 1 69 08 31 04, e-mail address: adrien.sari@cea.fr)

Abstract

This paper presents the investigation carried out by CEA List and ArcelorMittal R&D in order to assess the potential of linac-based neutron activation analysis to detect and quantify copper in scrap metal. Performances are evaluated using MCNP6 and then validated experimentally using a 6 MeV linac coupled with heavy water. It is shown that (γ, n) reaction cross-sections for deuterium are likely to be undervalued in ENDF/B-VII and suggested that photoneutron production algorithms in Monte Carlo codes should be reexamined.

Keywords: neutron activation; linac; scrap metal; copper; gamma spectrometry; HPGe detector.

1. Introduction

Detection and quantification of materials are widely required in many fields including, among others: archeology, biology, environmental sciences and industrial applications [1]–[5]. For this purpose, several instruments and methods can be deployed such as X-ray fluorescence (XRF) [6][7][8], inductively coupled plasma excitation with subsequent mass spectrometry (ICP-MS) [9], atomic absorption spectroscopy (AAS) [10], laser induced breakdown spectroscopy (LIBS) [11][12] and neutron activation analysis (NAA) [13][14]. Depending on the application foreseen, a measurement technique may be more adapted than others may. These techniques mainly differ by their detection limits, measurement time, and cost. Moreover, some techniques are more adapted to the characterization of large amount of materials whereas others are more adapted to measurements carried out on small amounts of materials. Some techniques enable surface interrogation (XRF, LIBS) whereas others allow for deeper interrogation (NAA). Some techniques require systematically chemical sample pre-treatment and separation of elements before analysis (AAS and ICP-MS) whereas others can provide online measurement (XRF, LIBS, NAA).

This paper presents the investigation carried out by CEA List and ArcelorMittal R&D with the aim of detecting and quantifying copper in scrap metal by linac-based neutron activation analysis. Detection and quantification of copper present in scrap metal is important as copper may cause two main problems in some metallurgy production and transformation processes. Roughly speaking, first, when copper is present the steel produced could be more breakable, which is not suitable for some particular uses of steel. Second, during some specific metallurgy processes, copper can migrate at the surface of the steel produced and lead to surface defects. NAA is a nuclear non-destructive technique, which enables identification and quantification of various elements without any chemical pretreatment. This technique allows for analysis of large amounts of materials and provides fast results thanks to online measurements in view of industrial applications. NAA is based on the use of a neutron source. A large variety of neutron sources exists: nuclear reactors [15]; isotopic sources like ^{252}Cf and ^{241}Am/Be; neutron generators based on deuterium–deuterium (D–D) and deuterium–tritium (D–T) fusion reactions; and linear electron accelerators (linac) coupled with a secondary target which converts high-energy photons to photoneutrons by (γ, n) reactions. The second target is usually made of beryllium [16] or heavy water (D_2O) [17] as ^{9}Be and deuterium have respectively (γ, n) reaction energy thresholds at 1.67 MeV and 2.2 MeV. For this work, neutron activation analysis will be performed at the SAPHIR platform (CEA Saclay, France) using a Linatron-M9 linac coupled with a heavy water secondary target. A linac-based setup enables to perform both neutron activation and high-energy imaging, which could be useful to help the interpretation of copper measurements in scrap metal.

Natural copper is composed of 69.15 % of ^{63}Cu and 30.85 % of ^{65}Cu. Neutron activation of copper leads to the production of ^{64}Cu and ^{66}Cu by (n, γ) reactions. Table 1 presents the half-lives of these two isotopes and the main characteristics of their delayed gamma-ray emission (energies and intensities). In order to optimize the neutron activation measurement time, the detection of ^{64}Cu was not retained in this study regarding its long half-life. For this study, copper will be detected using the highest intensity gamma-ray emitted by ^{66}Cu at 1039.20 keV using gamma spectrometry [18] thanks to a High-Purity Germanium (HPGe) detector.

Isotope	Half-life	Gamma-ray energy (keV)	Intensity (%)
^{64}Cu	12.7 h	1345.77	0.47
^{66}Cu	5.12 min	1039.20	9.23
		833	0.22
		1332.50	0.0037
		1872.20	0.00023

Table 1. Main characteristics of ^{64}Cu and ^{66}Cu [19][20].

In this paper, we investigate the detection and quantification of copper in a 220-liter drum containing scrap metal by linac-based neutron activation analysis. First, we assess performances obtained based on Monte-Carlo simulations. The aims of this study are the following:

- development of a simulation model of the setup;
- preliminary assessment of performances by simulation;
- and optimization of the measurement protocol.

Secondly, we validate experimentally the optimized protocol at the SAPHIR platform. Finally, we compare simulation and experimental results. The validity of the simulation model and discrepancies obtained will be presented and discussed.

2. Performance assessment based on Monte-Carlo simulations

2.1 Main building blocks

This multi-parametric study is based on Monte-Carlo simulations conducted with MCNP6.2 [21]. The setup is composed of a Linatron-M9 linac (designed by VARIAN, now renamed VAREX Imaging) operated at 6 MeV. Electrons are converted to high-energy photons by *Bremsstrahlung* thanks to a conversion target made of tungsten. High-energy photons are then converted to photoneutrons by (γ, n) reactions using a secondary target made of 16 kg of heavy water, which is placed at 45 cm from the linac tungsten conversion target and in a polyethylene measurement cell detailed in [22]. A 220-liter cylindrical drum of 82 cm (H) × 28.7 cm (r) containing a 1 g/cm^3 scrap metal matrix is positioned in the measurement cell and outside of the high-energy photon beam in order to be irradiated by neutrons thermalized in the cell. The chemical and isotopic compositions of the steel envelope of the drum are given in Table 2. The density of the steel envelope is 7.9 g/cm^3. The scrap metal matrix is simulated as pure natural iron as the precise chemical composition of this volume of material is unknown. The drum includes three channels in which a pure copper sample can be placed: at the center; in the periphery; and in the middle of the two latter positions. Fig. 1 shows a view of these different building blocks simulated with MCNP6.

Element	Weight percentages per element (%)	Isotope	Weight percentages per isotope (%)
Carbon	0.03	^{nat}C	0.03
Nitrogen	0.11	^{14}N	0.11
		^{15}N	Traces
Silicon	1.00	^{28}Si	0.92
		^{29}Si	0.05
		^{30}Si	0.03

Phosphorus	0.05	^{31}P	0.05
Sulphur	0.02	^{32}S	0.01
		^{33}S	Traces
		^{34}S	Traces
		^{36}S	Traces
Chromium	19.00	^{50}Cr	0.83
		^{52}Cr	15.92
		^{53}Cr	1.81
		^{54}Cr	0.45
Manganese	2.00	^{55}Mn	2.00
Iron	66.80	^{54}Fe	3.90
		^{56}Fe	61.29
		^{57}Fe	1.42
		^{58}Fe	0.19
Nickel	11.00	^{58}Ni	7.49
		^{60}Ni	2.89
		^{61}Ni	0.13
		^{62}Ni	0.40
		^{64}Ni	0.10

Table 2: Chemical and isotopic compositions of the steel envelope of the drum simulated with MCNP6.

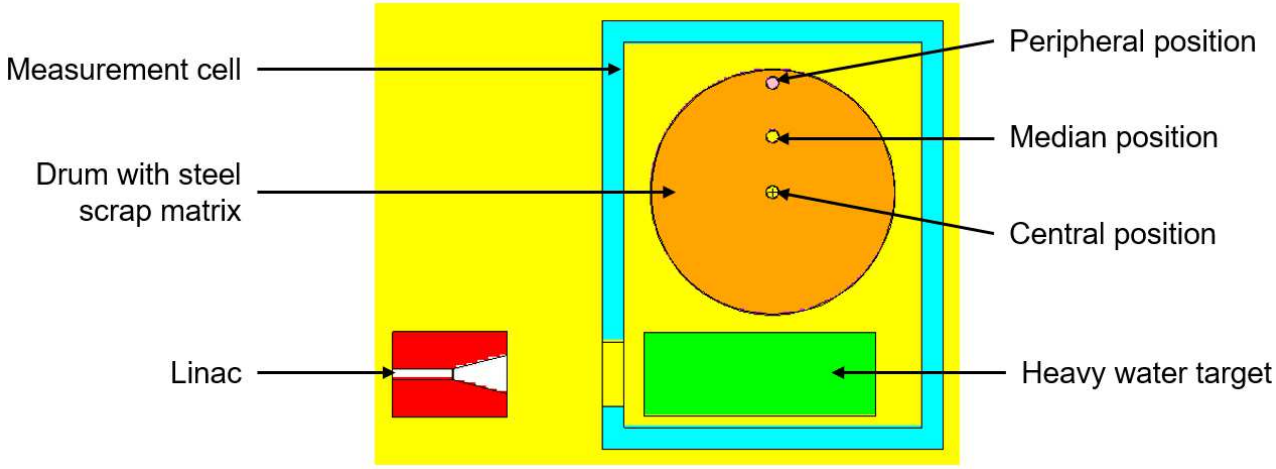

Fig. 1. Different building blocks of the setup simulated with MCNP6 and viewed with Vised [23].

MCNP6 simulations conducted in the frame of this study are carried out in three steps. First, we simulate the 6 MeV electron source of the linac and calculate both the neutron current on the way out of the six surfaces of the heavy water target and the neutron energy spectrum. The neutron current is 1.79×10^{-5} neutrons per electron and the energy spectrum is shown in Fig. 2. Exactly the same neutron current and energy spectrum were obtained using either one or the other of the two photonuclear data libraries available in MCNP6.2 for deuterium, that is to say “endf7u” or “la150u”.

Photoneutrons can interact by elastic scattering reactions on ^{16}O contained in the heavy water target. The (n, elastic) reaction cross-sections in ENDF/B-VII present peaks on the order of a few barns at around 0.4, 1.0, 1.3, 1.65, 1.85 and 1.9 MeV, which leads to dips at the same energies in the neutron energy spectrum. To a lesser extent, with lower cross-sections, (n, γ) reactions on ^{16}O may also occur and contribute marginally to the dips observed at around 0.4, 1.0, 1.65 and 1.85 MeV.

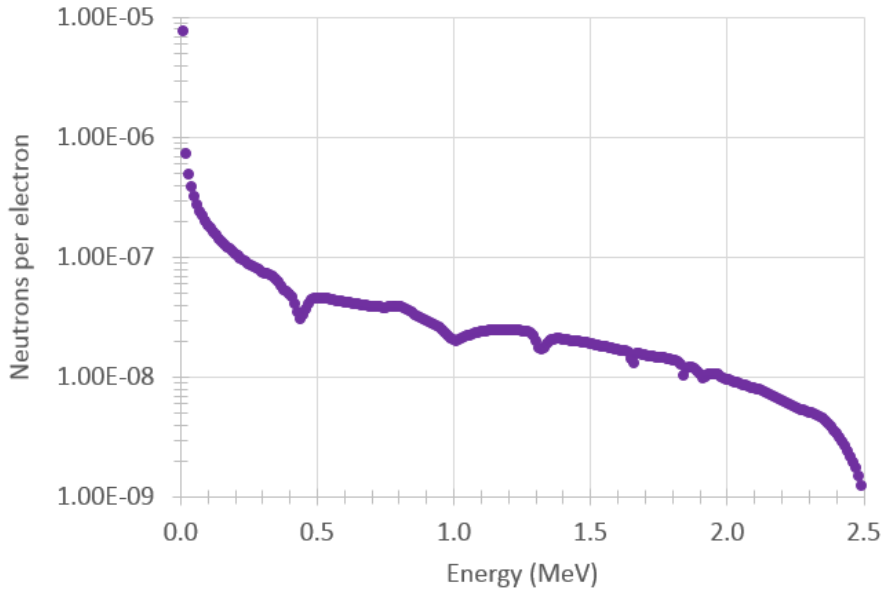

Fig. 2. Energy spectrum of photoneutrons emitted by the heavy water target and simulated with MCNP6.

Secondly, we simulate the production of photoneutrons in the heavy water secondary target taking into account an isotropic angular distribution and the energy spectrum determined previously, and calculate the rate of radiative captures of these neutrons on ^{65}Cu in the sample of natural copper. For these calculations, various masses of natural copper from 125 g to 1253.5 g were successively considered in the three sample positions. Copper was simulated as 100% of ^{65}Cu to calculate the (n, γ) reaction rates on ^{65}Cu exclusively (the impact of ^{63}Cu on the neutron flux is secondary in this simulation study).

Third, we simulate the 1039.20 keV gamma-ray emitted by the activated copper sample (^{66}Cu) and calculate the absolute detection efficiency of the HPGe detector (CANBERRA GR2021 model, which presents a relative detection efficiency of 20%). As can be seen in Fig. 3, the HPGe detector is placed at 1 cm from the drum through an opening located on the side of the cell once the plug removed.

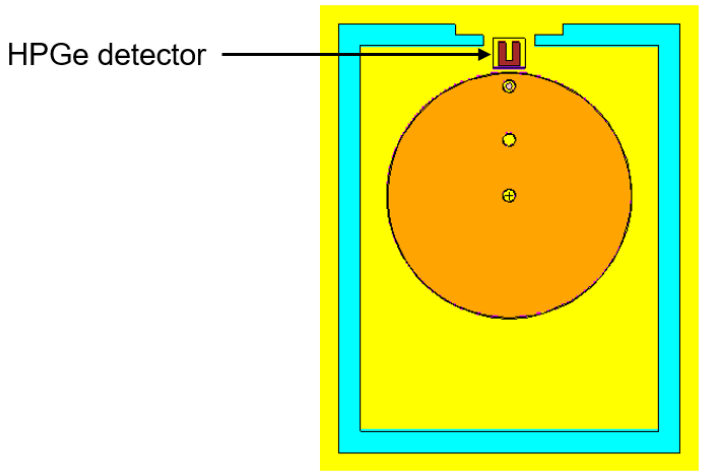

Fig. 3. Detection step simulated with MCNP6 and viewed with Vised [23].

2.2 Neutron flux characterization

The neutron flux at the three sample positions in the drum was characterized by MCNP6 simulation according to two parameters: the neutron current and the neutron energy spectrum. These two parameters were calculated using F1 tallies at the surface of each channel, also considering 1 meV energy bins to evaluate the energy spectra. Table 3 gathers the neutron currents obtained and Fig. 4 shows the probability density functions of the neutron current obtained by normalizing the neutron energy spectra obtained with MCNP6.

Position	Neutron current (neutrons per source neutron)
Peripheral	1.09×10^{-2}
Median	1.55×10^{-2}
Central	2.67×10^{-2}

Table 3. Neutron currents at the three positions in the drum.

The neutron current decreases from the central to peripheral positions. Indeed, we can see that the neutron current is reduced by a factor of approximately two between the central and the peripheral positions. This

result is consistent with the position of the heavy water secondary target in the cell with respect to the drum.

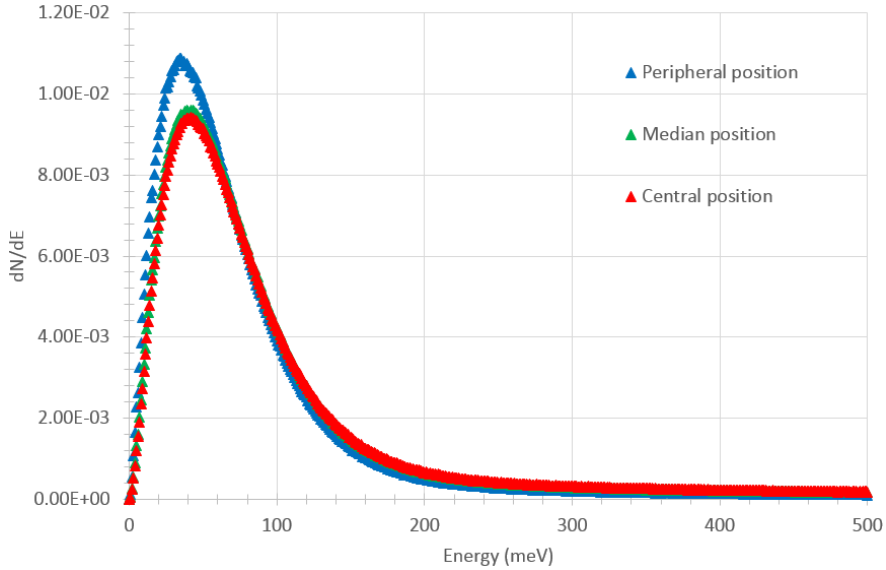

Fig. 4. Normalized neutron energy spectra at the three positions in the drum.

A hardening of the neutron energy spectrum is observed from the peripheral to the central position. The most probable neutron energies are respectively of 34 meV at the peripheral position and 42 meV at the central position. Moreover, it can be noticed that the tail of the energy spectrum above 70 meV is shifted to the right from the peripheral to the central position. This result could be explained by two phenomena:

- exposure to the fast neutron current, which decreases from the central to the peripheral position, due to the position of the heavy water secondary target in the cell with respect to the drum;
- absorption of thermal neutrons in the scrap metal matrix of the drum, which increases from the peripheral to the central position.

2.3 Calibration of the HPGe detector MCNP6 model

In order to calibrate the MCNP6 model of the HPGe detector, we compare detection efficiencies obtained by simulation and experiment in view of determining a correction factor for simulated detection efficiencies. The measurement consisted in acquiring a gamma spectrum during 20 minutes using three gamma sources: ^{137}Cs (428 kBq), ^{60}Co (454 kBq), ^{152}Eu (387 kBq), positioned at 50 cm from the HPGe

detector window. The two detection efficiency curves obtained by simulation and measurement are presented in Fig. 5.

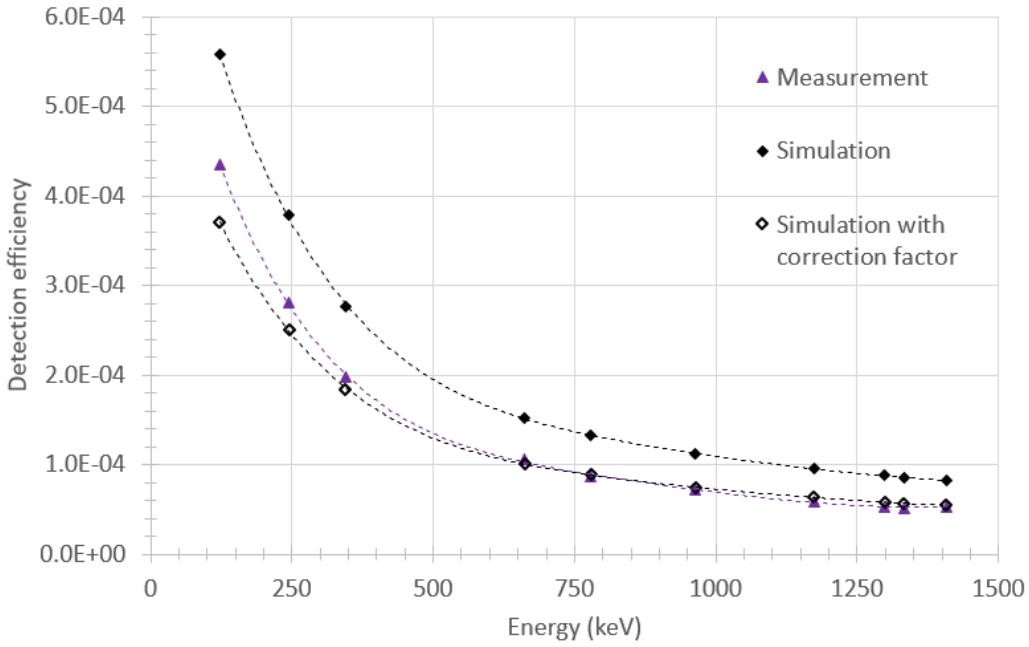

Fig. 5. Detection efficiency curves of the HPGe detector obtained by simulation and measurement.

The two detection efficiency curves obtained by simulation and measurement have similar trends on all the energy range considered from 121.78 keV to 1408.01 keV. However, simulation overestimates experiment by an average factor of 1.505 on this energy range. This correction factor will be used in the following of this study to correct detection efficiencies determined by simulation. The simulated detection efficiency curve taking into account this correction factor is also shown in Fig. 5. Above 500 keV, the average residual discrepancy between the corrected simulation curve and the experimental one is close to 6%.

2.4 Calculation methodology

In this study, the physical quantity of interest is the net peak area at 1039.20 keV in the gamma-ray spectrum. This quantity is calculated using the following formula:

$$\mathcal{A}_\gamma = \tau_{(n,\ \gamma)}\ \varepsilon_\gamma\ I_\gamma \frac{1 - e^{-n\lambda T}}{1 - e^{-\lambda T}} t_1\ e^{-\lambda t_2}\ (1$$

With:

- $\mathcal{A}_\gamma$: the net peak area (counts);

- $\tau_{(n,\ \gamma)}$: the $(n,\ \gamma)$ reaction rate on ^{65}Cu (number of reactions per second);
- ε_γ: the corrected detection efficiency of the HPGe detector (see section 2.3);
- I_γ: the emission intensity of the gamma-ray of interest (in %);
- n: the number of pulses during the irradiation;
- λ: the decay constant of the radioactive nucleus (in seconds^{-1});
- T: the pulse period (in seconds);
- t_1: the pulse duration (in seconds);
- t_2: the cooling time (in seconds);
- t_3: the counting time (in seconds).

In this formula, the $(n,\ \gamma)$ reaction rate on ^{65}Cu $\tau_{(n,\ \gamma)}$ and the corrected detection efficiency ε_γ of the HPGe detector are determined by MCNP6 simulation using respectively F4 and F8 tallies. Other terms of the equation either depending on the experimental protocol or extracted from nuclear database [20] are reported in the Table 4. We can emphasize on the fact that the linac pulse frequency is 200 Hz and that the irradiation time is set at 20 minutes. The irradiation time (t_3) is also the product between the number of pulses (n) and the pulse period (T).

Parameters	Values
I_γ	9.23 %
λ	2.27×10^{-3} s^{-1}
n	240000 pulses
T	5.00×10^{-3} s
t_1	2.50×10^{-6} s
t_2	120 s
t_3	1200 s

Table 4: Terms of the equation either depending on the experimental protocol or extracted from nuclear database.

2.5 Results and discussion

First, the evolution of the (n, γ) reaction rate on ^{65}Cu in the sample of natural copper and the evolution of the corrected gamma detection efficiency of the HPGe detector at 1039.20 keV were studied individually as a function of the natural copper mass considering the three sample positions. Results obtained are plotted respectively in Figs. 6 and 7.

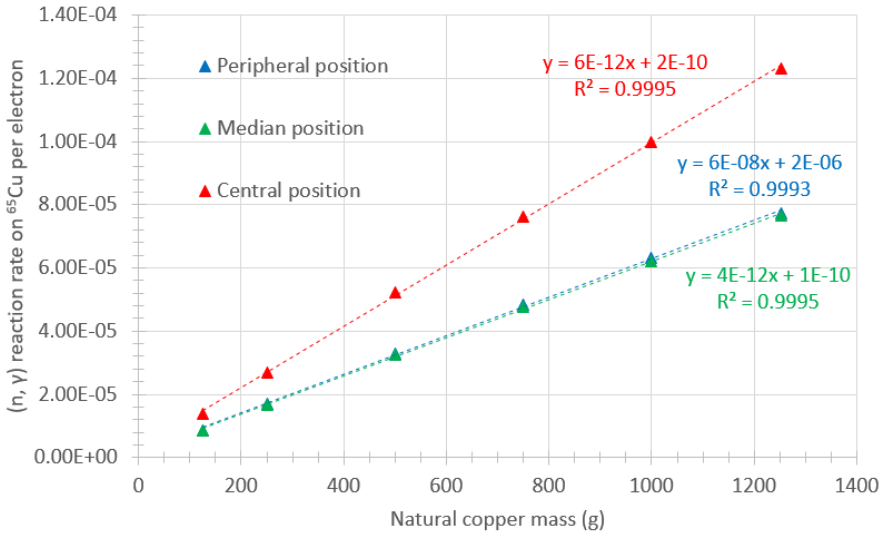

Fig. 6. (n, γ) reaction rate on ^{65}Cu as a function of the natural copper mass considering the three sample positions.

Whatever the position of the sample, the (n, γ) reaction rate on ^{65}Cu per electron as a function of the natural copper mass follows a linear trend. In addition, considering a given natural copper mass, the curves of the (n, γ) reaction rate on ^{65}Cu per electron for the sample placed in either the median or the peripheral position overlie on each other, and the sample is in average 1.58 times more activated when positioned in the central position. These results enable to determine the impact of the neutron flux characteristics, which were studied previously according to the three positions in the drum, on activation of the copper sample.

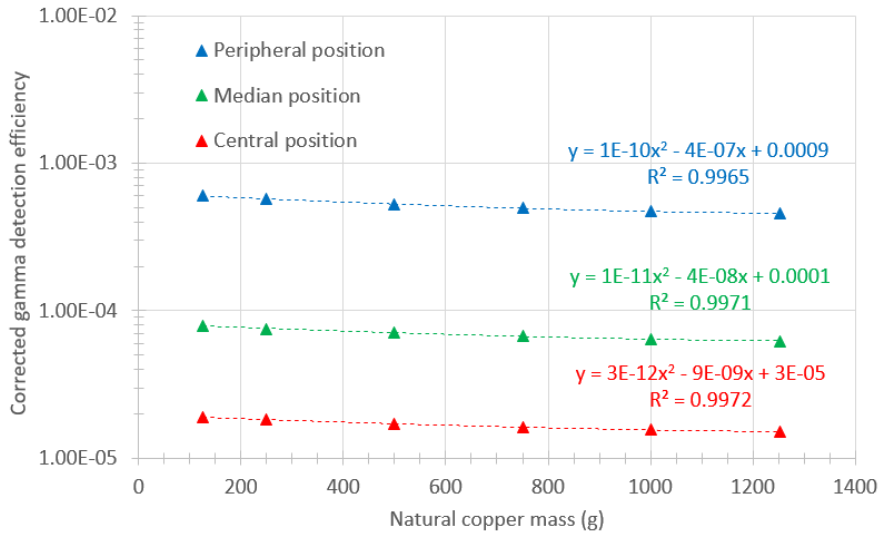

Fig. 7. Corrected gamma detection efficiency of the HPGe detector at 1039.20 keV as a function of the natural copper mass considering the three sample positions.

The corrected gamma detection efficiencies in the three sample positions as a function of the natural copper mass follow similar tendencies. In addition, considering a given copper mass, the detection efficiency is drastically degraded from the peripheral to the central position. For instance, the detection efficiency is approximately 30 times higher in the peripheral position compared to the central position. From results presented in the two previous figures, we can conclude that the gamma detection efficiency (detection step) is more dependent on the position of the copper sample than the (n, γ) reaction rate on ^{65}Cu (irradiation step).

The net peak area were then calculated, using the formula introduced previously, for the three sample positions and for various natural copper sample masses. Results obtained are presented in Fig. 8.

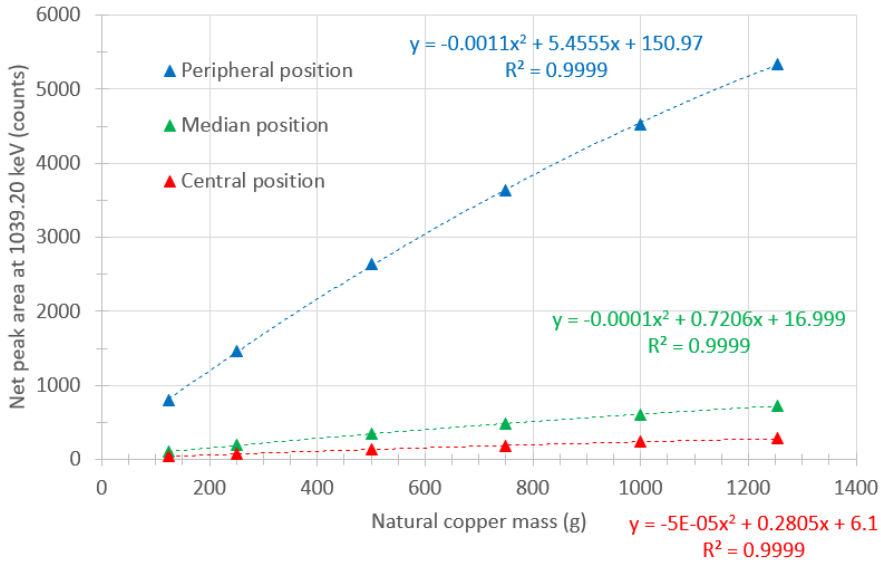

Fig. 8. Simulated net peak area at 1039.20 keV as a function of the natural copper mass considering the three sample positions.

The three curves show an increase of the net peak area with the natural copper mass following polynomial tendencies. Considering a given sample position, the net peak area increases by a factor higher than five when the copper mass increases from 125 g to 1253.5 g. As expected from our previous conclusions, the net peak area is higher when the sample is placed in the peripheral position. For instance, the net peak area is about 20 times higher when the sample is placed in the peripheral position rather than in the central position.

3. Experimental validation at the SAPHIR platform

In order to validate experimentally the performances of the setup simulated previously, measurements were carried out at the SAPHIR platform (CEA Saclay, France) [24], [25]. The irradiation step of the neutron activation measurement, shown in Fig. 9, involves an M9-Linatron linac (operated at 6 MeV and at 200 Hz during 20 minutes), and a secondary target of 16 kg of heavy water placed in a polyethylene cell [22]. The average neutron emission intensity, estimated based on MCNP6 simulation, reaches 5.6×10^{9} neutrons per second. In this figure, we can also notice the 220 liter drum containing the 1 g/cm^3 scrap metal matrix and its three channels in which copper samples may be inserted. The copper samples consist in an assembly of 80 cm long copper wires of 99.95+% purity.

During the two minutes of cooling time, the HPGe detector (GR2021 CANBERRA) is brought in position at mid-height of the drum and at a distance of 1 cm through an opening located on the side of the cell, as shown in Fig. 10. It is important to emphasize that, during each irradiation, the neutron cell is totally closed and that the HPGe detector is far from the cell to avoid irradiation of the latter. The gamma spectrum acquisition time is set at 20 minutes. These acquisitions are performed by the means of a CAEN Hexagon multichannel analyser and pulse processor [26]. An example of the peak of interest at 1039.20 keV in the gamma spectrum is given in Fig. 11. The background was measured with the same measurement protocol as the one detailed previously but without any sample of copper in the drum.

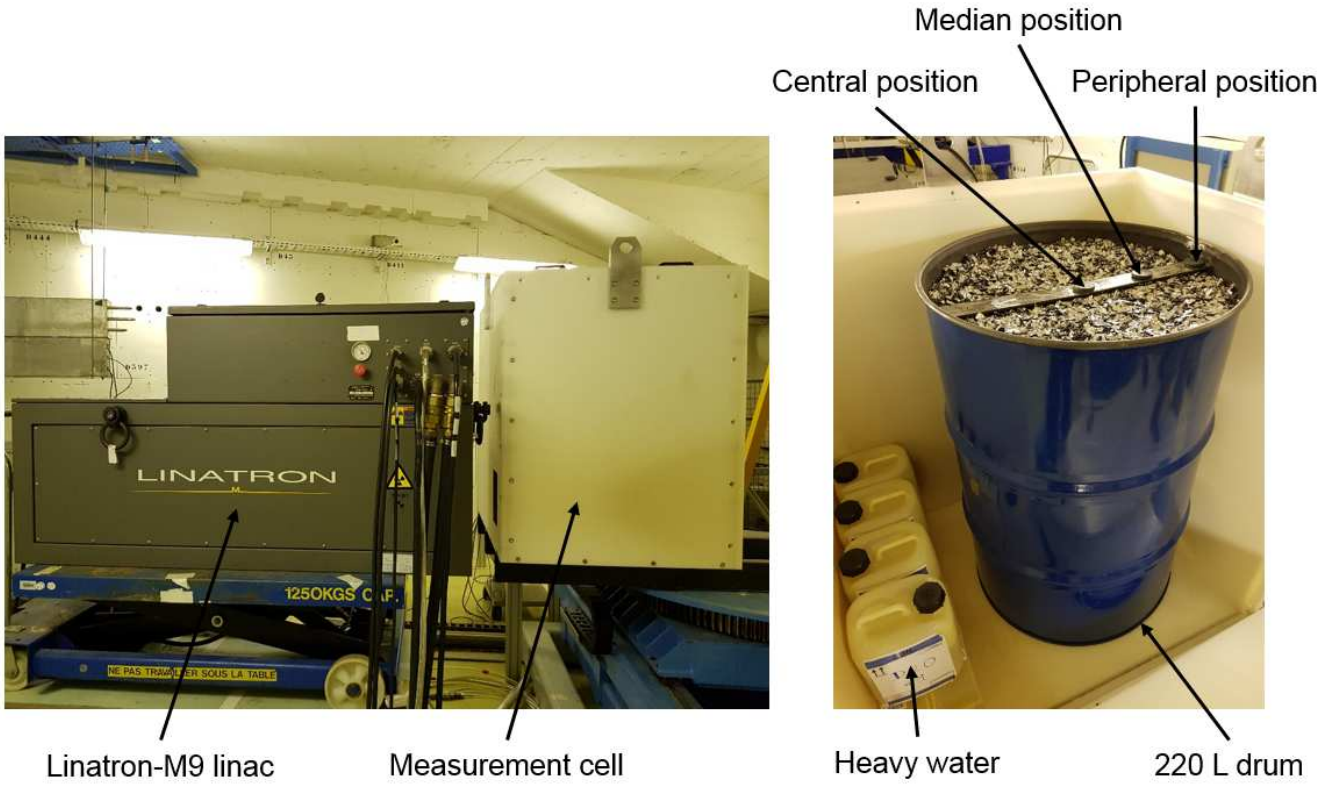

Fig. 9. Irradiation step of the neutron activation measurement.

Fig. 10. Detection step of the neutron activation measurement.

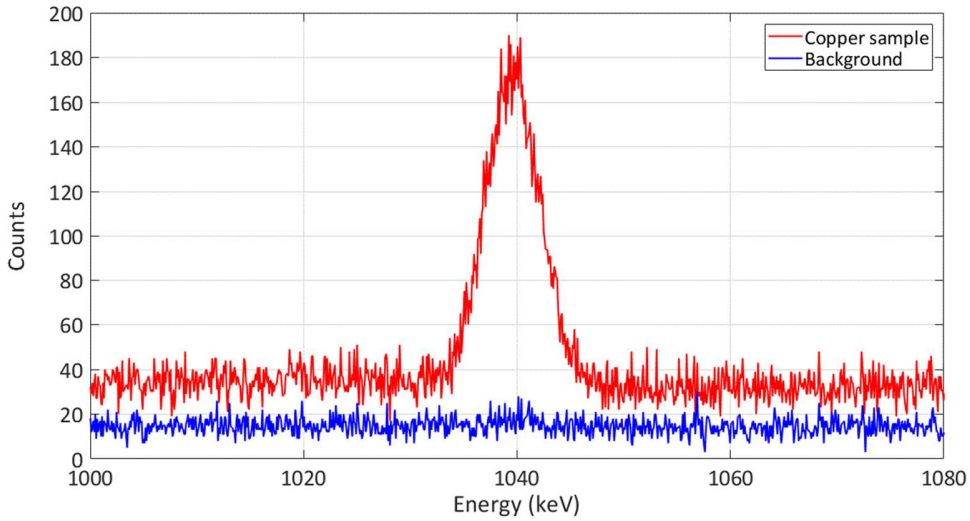

Fig. 11. Example of the peak of interest at 1039.20 keV in the gamma spectrum obtained for a sample of natural copper of 1253.5 g activated in the peripheral position of the drum.

The net peak areas obtained experimentally as a function of the copper mass considering the peripheral and median positions are plotted in Fig. 12. Indeed, the signal obtained in the central position was not statistically significant.

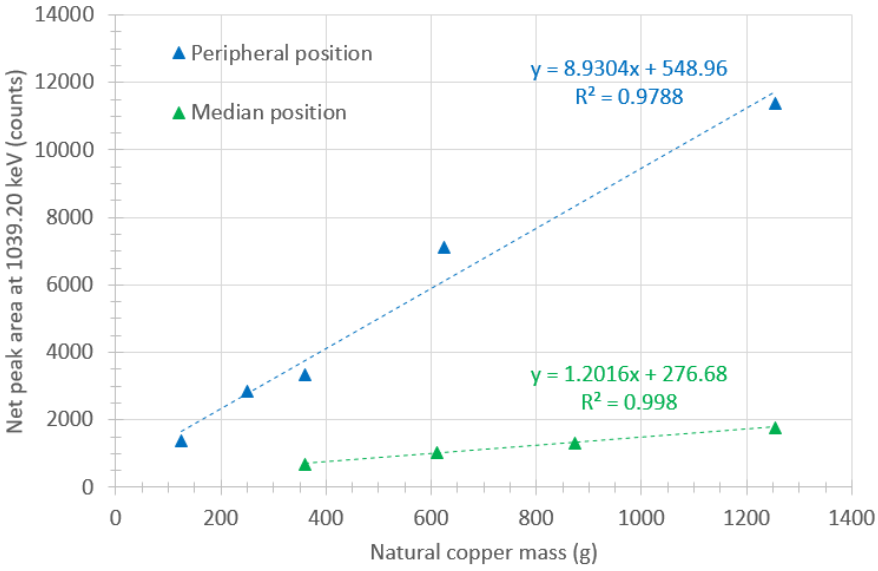

Fig. 12. Measured net peak area at 1039.20 keV as a function of the natural copper mass considering the three sample positions.

As we can see, measurements carried out enabled to elaborate calibration curves (net peak area as a function of the copper mass) for the peripheral and median positions. The two curves obtained show linear trends. As expected from results of the simulation study, the net peak area is in average six times higher for the copper sample placed in the peripheral position than in the median position. We can also notice that under 360 g of copper, the net peak area measured is not statistically significant when the sample is placed in the median position of the drum. Consequently, mass detection limits calculations were performed in order to determine the limits of this measurement setup in the frame of the detection of natural copper by neutron activation. Table 5 gathers mass detection limits estimated [27].

Sample position	Mass detection limit (g)
Peripheral	39
Median	249

Table 5. Mass detection limits of natural copper estimated in the peripheral and median positions of the drum.

The mass detection limit is lower by a factor of six when the sample is placed in the peripheral position rather than in the median position of the drum. These results can be interpreted thanks to simulation results obtained in section 2. Indeed, the mass detection limit is inversely proportional to the detection efficiency. This latter parameter — which has the stronger impact when the copper sample changes from one position to another in the drum — decreases considerably from the peripheral to the median position. Moreover, it is interesting to emphasize that, as various elements and traces of copper are present in the scrap metal matrix, activation of the latter leads to a stronger background, which contributes to increase the mass detection limit.

4. Comparison between simulation and experimental results

Further to the assessment of performances based on MCNP6 simulation (section 2) and the experimental study conducted at the SAPHIR platform (section 3), we can now compare and study discrepancies

obtained between simulation and experimental results. For this purpose, the net peak area at 1039.20 keV in the gamma spectrum, due to ^{66}Cu, obtained for the 1253.5 g copper sample are reported in Table 6.

Sample position	Simulation	Measurement	$\frac{Simulation}{Measurement}$
Peripheral	5345 ± 73	11386 ± 107	0.47 ± 0.01
Median	723 ± 27	1780 ± 42	0.41 ± 0.02

Table 6. Comparison between simulated and experimental net peak areas at 1039.20 keV obtained for a sample of natural copper of 1253.5 g.

Simulation underestimates experiment roughly by a factor of two when the linac is operated at 6 MeV, which corroborates results obtained in the frame of a previous study [25]. Indeed, the photonuclear cross-sections of the (γ, n) reaction on deuterium could potentially be undervalued in the ENDF/B-VII database [28], which could lead to an underestimated neutron production by the heavy water secondary target by simulation. Nevertheless, algorithms used to simulate photoneutron production should also be carefully reexamined as the latter could also be involved in the errors brought to light. Anyhow, these new results are in line with the prior conclusion according to which the photoneutron production of a heavy water secondary target coupled with a linac in the same electron energy range should be carefully evaluated.

As the gap between simulated and experimental results can be quantified, the MCNP6 simulation model of the setup is reliable and its use could be extended to the detection and characterization of other elements than copper. In other words, this study shows that reliable simulation models can be achieved and used for further developments of linac-based neutron activation techniques.

5. Conclusion and outlook

In this study, CEA List and ArcelorMittal R&D investigated the potential of linac-based neutron activation analysis to detect and quantify copper in scrap metal. For this purpose, we assessed performances obtained by Monte-Carlo simulation using the MCNP6 code and ENDF/B-VII nuclear data libraries. Both the irradiation and detection steps of the measurement were simulated. The neutron flux was characterized according to two parameters: the neutron current and the neutron energy spectrum at each of the three sample positions in the drum. Then, the MCNP6 simulation model of the HPGe detector was calibrated experimentally and enabled to determine a correction factor of 1.505 on simulated detection efficiencies. Once the calculation methodology described, the evolution of the (n, γ) reaction rate on ^{65}Cu and the HPGe gamma detection efficiency were both studied as a function of the natural copper mass considering the three sample positions. It has been highlighted that the gamma detection efficiency (detection step) is more dependent on the position of the copper sample than the (n, γ) reaction rate on ^{65}Cu (irradiation step). These two parameters were then used for the calculation of the quantity of interest: the net peak area at 1039.20 keV in the gamma spectrum. For a given natural copper mass, the net peak area is higher when getting closer to the peripheral position in the drum, thus showing that the peripheral position is more favorable to the detection of copper.

In order to validate experimentally the performances of this setup, measurements were carried out at the SAPHIR platform. These measurements enabled to elaborate calibration curves (net peak area at 1039.20 keV as a function of the natural copper mass) for the peripheral and median positions. Mass detection limits of 39 g and 249 g of natural copper were then estimated respectively in the peripheral and the median positions. Subsequently, comparison between simulated and experimental results brought to light discrepancies by a factor of two approximately when the linac is operated at 6 MeV, which corroborates a prior conclusion according to which the photonuclear cross-sections of the (γ, n) reaction on deuterium are likely to be undervalued in the ENDF/B-VII database. Nevertheless, photoneutron production algorithms in Monte Carlo codes should also be carefully reexamined.

This work enabled to develop and validate a reliable MCNP6 simulation model that could be extended to the detection and characterization of other elements than copper. Moreover, this study shows that reliable simulation models can be achieved and used for further developments of linac-based neutron activation techniques. In addition, as calibration curves are significantly different for various sample positions, developments towards activated sample localization techniques are currently under investigation.

Funding

This work was supported by ArcelorMittal, Global Research and Development.

References

[1] K. Melessanaki, M. Mateo, S. C. Ferrence, P. P. Betancourt, and D. Anglos, "The application of LIBS for the analysis of archaeological ceramic and metal artifacts," in *Applied Surface Science*, 2002.

[2] M. C. Cantone *et al.*, "Proton, photon and neutron activation analysis for the determination of stable isotopes of gadolinium in human blood plasma," *J. Radioanal. Nucl. Chem.*, 2000.

[3] T. Kato, N. Sato, and N. Suzuki, "Non-destructive multi-element photonactivation analysis of environmental materials," *Talanta*, 1976.

[4] T. M. de Lima, D. C. Weindorf, N. Curi, L. R. G. Guilherme, R. M. Q. Lana, and B. T. Ribeiro, "Elemental analysis of Cerrado agricultural soils via portable X-ray fluorescence spectrometry: Inferences for soil fertility assessment," *Geoderma*, 2019.

[5] A. Sari *et al.*, "The Potential of Photon Activation and Neutron Activation Techniques for Fast Soil Characterization," *EPJ Web Conf.*, vol. 225, p. 09001, Jan. 2020.

[6] R. D. Irons, E. A. Schenk, and R. D. Giauque, "Energy dispersive X ray fluorescence spectroscopy and inductively coupled plasma emission spectrometry evaluated for multielement analysis in complex biological matrices," *Clin. Chem.*, 1976.

[7] E. K. Towett, K. D. Shepherd, and B. Lee Drake, "Plant elemental composition and portable X-ray fluorescence (pXRF) spectroscopy: Quantification under different analytical parameters," *X-Ray Spectrom.*, 2016.

[8] L. Musílek, T. Čechák, and T. Trojek, "X-ray fluorescence in investigations of cultural relics and archaeological finds," *Appl. Radiat. Isot.*, 2012.

[9] H. J. Van De Wiel, "Determination of elements by ICP-AES and ICP-MS," *Natl. Inst. Public Heal. Environ. (RIVM)*, 2003.

[10] T. Stafilov and I. Karadjova, "Atomic absorption spectrometry in wine analysis," *Maced. J. Chem. Chem. Eng.*, 2009.

[11] M. A. Gondal and M. N. Siddiqui, "Identification of different kinds of plastics using laser-induced breakdown spectroscopy for waste management," *J. Environ. Sci. Heal. - Part A Toxic/Hazardous*

Subst. Environ. Eng., 2007.

[12] L. Bassel *et al.*, "Laser-induced breakdown spectroscopy for elemental characterization of calcitic alterations on cave walls," *Environ. Sci. Pollut. Res.*, 2017.

[13] A. El-Taher and M. A. K. Abdelhalim, "Elemental analysis of limestone by instrumental neutron activation analysis," *J. Radioanal. Nucl. Chem.*, 2014.

[14] A. Ashraf *et al.*, "Rare earth elements in core marine sediments of coastal East Malaysia by instrumental neutron activation analysis," *Appl. Radiat. Isot.*, 2016.

[15] B. Canion and S. Landsberger, "Determining trace amounts of nickel in plant samples by neutron activation analysis," in *Journal of Radioanalytical and Nuclear Chemistry*, 2013.

[16] F. Jallu *et al.*, "Simultaneous neutron and photon interrogation method for fissile and non-fissile element separation in radioactive waste drums," *Nucl. Instruments Methods Phys. Res. Sect. B Beam Interact. with Mater. Atoms*, 2000.

[17] L. Lakosi and C. T. Nguyen, "Neutron interrogation of high-enriched uranium by a 4 MeV linac," *Nucl. Instruments Methods Phys. Res. Sect. B Beam Interact. with Mater. Atoms*, 2008.

[18] G. R. Gilmore, *Practical Gamma-ray Spectrometry*, Second Edi. pp. 131-141, 2008.

[19] M. Bé, V. Chisté, C. Dulieu, V. Chechev, N. Kuzmenko, and M. Galán, *BIPM monography 5*. 2010.

[20] D. A. Brown *et al.*, "ENDF/B-VIII.0: The 8th Major Release of the Nuclear Reaction Data Library with CIELO-project Cross Sections, New Standards and Thermal Scattering Data," *Nucl. Data Sheets*, 2018.

[21] C. J. Werner *et al.*, "Title: MCNP Version 6.2 Release Notes," *LA-UR-18-20808*, 2018.

[22] A. Sari, F. Carrel, F. Lainé, and A. Lyoussi, "Design of a neutron interrogation cell based on an electron accelerator and performance assessment on 220 Liter nuclear waste mock-up drums," *IEEE Trans. Nucl. Sci.*, 2014.

[23] R. Schwarz, A. Schwarz, and L. Carter, "Wizards and visualization features for MCNP geometries and sources," in *American Nuclear Society's 14th Biennial Topical Meeting of the Radiation Protection and Shielding Division*, 2006.

[24] F. Carrel, M. Agelou, M. Gmar, F. Lainé, B. Poumaréde, and B. Rattoni, "Measurement of plutonium in large concrete radioactive waste packages by photon activation analysis," *IEEE Trans. Nucl. Sci.*, 2010.

[25] A. Sari, F. Carrel, and F. Lainé, “Characterization and Optimization of the Photoneutron Flux Emitted by a 6- or 9-MeV Electron Accelerator for Neutron Interrogation Measurements,” *IEEE Trans. Nucl. Sci.*, 2018.

[26] “Hexagon,” *https://www.caensys.com*. .

[27] G. R. Gilmore, *Practical Gamma-Ray Spectrometry*, Second Edi. pp. 117, 2008.

[28] M. B. Chadwick *et al.*, “ENDF/B-VII.0: Next Generation Evaluated Nuclear Data Library for Nuclear Science and Technology,” *Nucl. Data Sheets*, 2006.